

Resonant optomechanics with a vibrating carbon nanotube and a radio-frequency cavity

N. Ares,¹ T. Pei,¹ A. Mavalankar,¹ M. Mergenthaler,¹ J.H. Warner,¹ G.A.D. Briggs,¹ and E.A. Laird¹

¹*Department of Materials, University of Oxford, Parks Road, Oxford OX1 3PH, United Kingdom*

(Dated: October 24, 2016)

In an optomechanical setup, the coupling between cavity and resonator can be increased by tuning them to the same frequency. We study this interaction between a carbon nanotube resonator and a radio-frequency tank circuit acting as a cavity. In this resonant regime, the vacuum optomechanical coupling is enhanced by the DC voltage coupling the cavity and the mechanical resonator. Using the cavity to detect the nanotube's motion, we observe and simulate interference between mechanical and electrical oscillations. We measure the mechanical ring-down and show that further improvements to the system could enable measurement of mechanical motion at the quantum limit.

The field of cavity optomechanics exploits resonant enhancement of light-matter interaction to study mechanical motion with exquisite sensitivity, including in the quantum domain [1]. Commonly the mechanical frequency f_M is much smaller than the frequency f_E of the electromagnetic cavity, leading to a detuned coupling. The small zero-point motion then gives a comparatively weak optomechanical coupling, which however can be enhanced by a factor $\sqrt{n_c}$ through strong driving, where n_c is the cavity photon occupation [2]. An alternative approach, which avoids the degradation of the cavity performance at low-temperatures for large n_c [3], is to operate close to resonance, at $f_M \approx f_E$, with a DC voltage \bar{V}_G applied between the resonator and the cavity [4, 5]. In this case, the single-photon coupling is enhanced by a factor $\sim \bar{V}_G/V_{ZP}$, where V_{ZP} is the zero-point fluctuation of the cavity voltage [6]. However, for this scheme to approach the quantum regime, it requires a mechanical resonator with a frequency high enough to be thermalized close to its ground state.

Here we realize a resonant optomechanical circuit exploiting the high mechanical frequency of a vibrating carbon nanotube. Using a radio-frequency (RF) circuit as a readout cavity [7, 8], we detect nanotube motion via its changing capacitance and measure interference between electrical and mechanical resonances. We show that the cavity measurement reproduces the resonance observed in transport, but go beyond transport by measuring the ringdown even without current through the nanotube. We reproduce the behavior in simulations, and show that feasible improvements to detection would approach the quantum limit.

Vibrating nanotubes offer attractive properties including high quality factors, large quantum zero-point motion, and high frequencies such that dilution refrigeration approaches the zero-phonon limit [9–17]. This has allowed development of force and mass sensors [18–20], as well as proposals for coupling to electron spins [21, 22] and optical photons [23, 24]. A fiber cavity was recently used to detect room-temperature Brownian motion [25], but cryogenic measurements to date rely on electrical

transport through the nanotube, forgoing potential for sensitivity and coherent control offered by coupling to an chip-scale cavity.

A carbon nanotube resonator [Fig.1(a)] was suspended between contact electrodes over an array of five finger gates as described in Ref. [6, 26]. For transport measurements the device is probed by applying a bias V_{sd} and measuring the current I through the nanotube. The doping of the nanotube, and hence its conductance, are tuned using DC gate voltages \bar{V}_{G1} to \bar{V}_{G5} ; these simultaneously tune the mechanical tension [9]. We define \bar{V}_G as the DC voltage applied to all gate electrodes. Gate 4 is connected to an RF source that can be used to excite transverse vibrations. Measurements are at 13 mK in a dilution refrigerator.

The effective RF cavity is realized using an inductor and capacitors mounted on the sample holder and coupled to gate 5. To tune cavity frequency f_E , we incorporate a variable capacitor C_S controlled by a DC voltage V_S , giving $f_E \approx (2\pi\sqrt{LC_S})^{-1}$, where $L = 180$ nH is the circuit inductance [27]. This cavity can be driven in two ways; by injecting an RF signal to the input via a directional coupler (direct drive), and by driving via gate 4, which is capacitively coupled (gate drive). The cavity output is fed to a cryogenic amplifier and detected at room temperature. The entire setup forms a three-terminal circuit with input ports 1 and 2 and output port 3. Figure 1(b) shows electrical scattering parameters as a function of driving frequency f_d for two settings of V_S in both direct and gate drive. The cavity resonance is evident as a transmission minimum with quality factor $Q_E \approx 10 - 20$ depending on varactor losses [27].

The mechanical resonance is first studied in transport [Fig.1(c)] [9]. A hole-doped quantum dot potential is created through a combination of Schottky barriers at the contacts and a voltage \bar{V}_G . As a function of \bar{V}_G , a series of Coulomb peaks is evident in transport [Fig.1(c) inset]. The effect of mechanical displacement is to change the capacitance between the dot and the gates [13], shifting the Coulomb peaks in a way that leads to a rectified DC current I . With an RF signal applied to gate 4, this

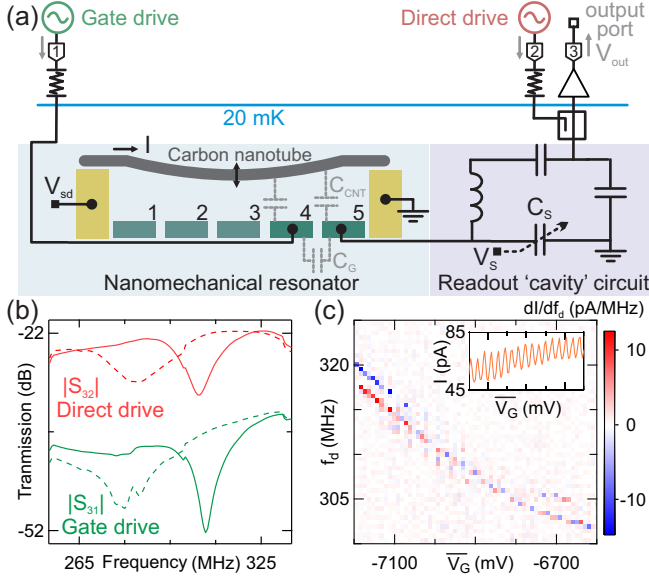


FIG. 1. (a) Experimental setup. A gated and contacted carbon nanotube resonator is connected to a radio-frequency tank circuit acting as a readout cavity. Nanotube motion is excited via a gate drive; the cavity can independently be probed directly via a directional coupler. The cavity response is detected via a cryogenic amplifier. The combined setup acts as a three-port RF device, with transmission measurements possible from ports 1 or 2 to port 3. Dotted capacitors indicate coupling between gates 4 and 5 and between these gates and the nanotube. DC voltages \bar{V}_{G1} to \bar{V}_{G3} are applied to gates 1-3. Bias tees (not shown) allow DC voltages \bar{V}_{G4} and \bar{V}_{G5} to be added to the RF signal on gates 4 and 5, respectively. (b) Transmission as a function of frequency with cavity tuning voltage $V_s = 9$ V (solid line) and $V_s = 0.2$ V (dotted line) for both direct and gate drive, showing a tuneable resonance. The different insertion losses are mainly due to different fixed attenuators in the two paths. (c) Numerically differentiated dI/df_d as a function of f_d and \bar{V}_G . The gate drive power was $P = -33$ dBm. Inset shows I over the same \bar{V}_G range with $V_{sd} = 10$ mV and with no RF excitation.

is evident when dI/df_d is plotted as a function of \bar{V}_G and f_d [13, 14, 16]. A resonance feature is seen at the mechanical frequency f_M [Fig. 1(c)]. The measured f_M is consistent with similar nanotube resonators [9–13, 15, 19]. The mechanical nature is clear from the dependence on \bar{V}_G due to electrostatic tensioning.

We now detect this motion via the readout cavity. The dependence of gate capacitance C_{CNT} on mechanical displacement u leads to a cavity coupling $\frac{df_E}{du} \approx \frac{f_E}{2C_s} \frac{\partial C_{CNT}}{\partial u}$ [6]. In a detuned optomechanical setup with $f_M \ll f_E$, this coupling allows the motion to be monitored via the phase shift of the cavity transmission [1, 3]. We use a different scheme that takes advantage of the fact that f_M and f_E can be tuned into resonance. With the DC voltage on gate 5 set to \bar{V}_G , the mechanical motion induces a current $I_G = -\bar{V}_G \frac{\partial C_{CNT}}{\partial u} \frac{du}{dt}$ onto the gate electrode. This current excites the cavity, leading to an

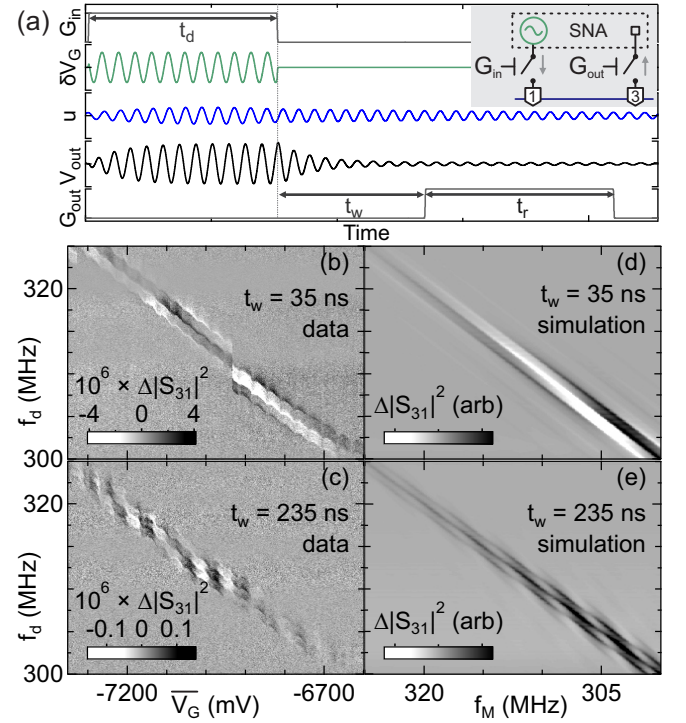


FIG. 2. (a) Schematic pulsed excitation and measurement scheme, showing gating signals G_{in} and G_{out} together with simulated drive δV_G , displacement u , and cavity output voltage V_{out} . Durations of drive (t_d), wait (t_w) and acquisition (t_r) are indicated. Inset: room-temperature gating scheme using RF switches. (b), (c) Time-averaged $\Delta|S_{31}|^2$, measured using the scheme in (a), as a function of \bar{V}_G and f_d for two different values of t_w . Each column of data is averaged for 5 s. Measurement parameters were $V_s = 9$ V, $V_{sd} = 2$ mV, $P = -38$ dBm and $t_d = t_r = 300$ ns. The jump at $\bar{V}_G \approx -6900$ mV indicates an electrostatic switcher in the device. (d), (e) Simulated $\Delta|S_{31}|^2$ (see text) reproducing panels (b) and (c) respectively.

output signal

$$V_{out} = Z_{trans} I_G, \quad (1)$$

where Z_{trans} is a transimpedance set by the circuit parameters [6]. The transimpedance, and hence the sensitivity, is maximal close to degeneracy ($f_M \approx f_E$). In contrast to detuned readout (at least outside the resolved-sideband regime), the signal arises from velocity $\frac{du}{dt}$ rather than displacement.

We demonstrate this coupling with the cavity tuned to $f_E = 304$ MHz and with $\bar{V}_G = -7$ V. Drive and detection are provided by a scalar network analyser (SNA), which monitors the time-average transmission $|S_{31}|$ from port 3 to port 1. A challenge of this scheme is that the drive used to actuate motion also couples directly to the cavity via a parasitic capacitance C_G between gates 4 and 5. This gives rise to a non-resonant background that in our unoptimized circuit overwhelms the mechanical signal. (This is why a mechanical signal is not seen directly in

Fig. 1(b)). We can largely reject this contribution using the pulsed driving scheme of Fig. 2(a), which separates the times of driving and detection using RF switches to gate the input and output signals. With the output decoupled, gate 4 is first driven for time $t_d = 300$ ns, exciting both the mechanical motion and the cavity voltage. After a wait interval t_w from the end of this drive burst, the output is coupled for a detection interval of duration $t_r = 300$ ns. For each data point, the detected power was averaged over ~ 8 ms during which this cycle was applied with a period of $t_w + 610$ ns. By choosing t_w intermediate between the cavity and mechanical ringdown times ($Q_E/2\pi f_E \approx 11$ ns $> t_w > Q_M/2\pi f_M \approx 370$ ns), the mechanical contribution to V_{out} is largely isolated.

Figure 2(b-c) shows transmission as a function of f_d and \bar{V}_G for two different values of t_w . To highlight the signal due to the nanotube, data are plotted after subtraction of the average $|S_{31}|^2$ at each frequency, giving the excess signal $\Delta|S_{31}|^2$. The mechanical resonance is evident, with a similar dependence of f_M on \bar{V}_G as measured in Fig. 1(c). However, it now appears as a pattern of bright and dark fringes whose alignment depends on t_w . This is attributable to a classical interference effect between the ringdown of mechanical and electrical signals. Both the nanotube and the cavity are set ringing during the drive burst with phases that depend on the difference between their corresponding resonance frequencies and f_d . Subsequently each evolves at its own frequency. The two signals therefore add constructively or destructively in a way that depends on t_w , f_d , f_E , and f_M (tuned by \bar{V}_G). Superimposed on this pattern are sidebands separated by the gating repetition frequency. The data also show a stairlike dependence of f_M on \bar{V}_G because Coulomb blockade modulates the electrostatic tensioning [28–30].

Both fringes and sidebands are reproduced in a simulation [6] of $V_{\text{out}}(f_M, f_d)$ by modelling the electrical and mechanical impedances between gate 4 and the cavity output [Fig. 1(c-d)]. From the sharpness of the resonance and the intensity of the interference fringes, the mechanical quality factor can be estimated as $Q_M \approx 700$, while the effective coupling is $\partial C_{\text{CNT}}/\partial u \sim 0.3 \times 10^{-12}$ Fm $^{-2}$, roughly consistent with the device geometry [6]. Coulomb blockade effects are not seen in the simulation because results are plotted as a function of f_M rather than \bar{V}_G .

In contrast to previous electromechanical measurements of nanotubes [9–15, 19], cavity readout allows detection of mechanical motion even for device configurations where I is unmeasurably small. To access such a configuration, we set $\bar{V}_{G2} = \bar{V}_{G3} = \bar{V}_{G4} = -7250$ mV and we adjust $\bar{V}_{G1} = \bar{V}_{G5} \equiv \bar{V}_{\text{TB}}$ to tune the dot tunnel barriers. Figure 3 inset shows how, as an increased \bar{V}_{TB} makes tunnel rates smaller, transport turns-off to an undetectable level ($I \ll 1$ pA) when $\bar{V}_{\text{TB}} \gtrsim 4000$ mV. As expected, the mechanical resonance becomes correspond-

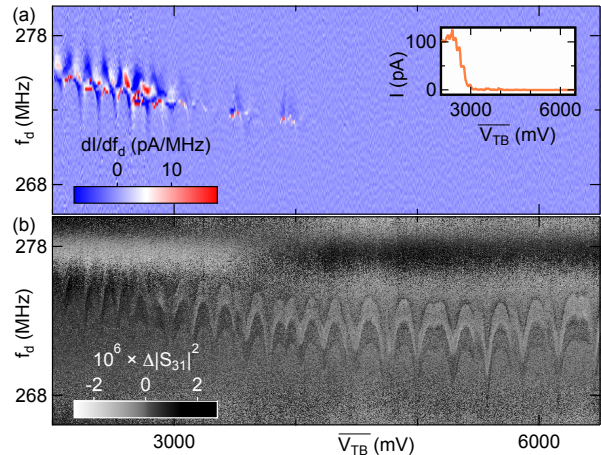


FIG. 3. (a) Numerically differentiated dI/df_d as a function of f_d and \bar{V}_{TB} for $P = -38$ dBm and $V_{\text{sd}} = 10$ mV. The inset shows I for the same range of \bar{V}_{TB} and same V_{sd} with no microwaves applied. As \bar{V}_{TB} increases, the tunnel barriers are pinched off so that I cannot be detected. (b) Measured $\Delta|S_{31}|^2$ following the scheme in Fig. 2(a) and plotted as a function of f_d and \bar{V}_{TB} . The resonance is seen even with transport pinched off. Measurement parameters were $V_S = 0.2$ V, $t_d = t_r = 300$ ns and $t_w \sim 15$ ns.

ingly unmeasurable in transport [Fig. 3(a)]. However, it is evident in cavity readout across the entire range [Fig. 3(b)]. The oscillations of f_M as a function of \bar{V}_{TB} are an effect of mechanical softening on Coulomb blockade peaks [29, 30] and indicate that the sum of the dot's tunnel rates to left and right, although not big enough to lead to a detectable current, is at least of the order of f_M ($\Gamma_L + \Gamma_R \gtrsim f_M$).

We now study the mechanical decay rate for different tunnel barrier configurations by directly measuring the ringdown. A time-resolved measurement was previously performed using a fast current amplifier [15], but relied on transport through the device. Since for some barrier configurations, Q_M is known to be limited by tunneling resistance [16, 17, 29, 30], it is of interest to determine the limiting Q_M in an electrically pinched-off nanotube. Extracting a precise linewidth from data as in Fig. 2 is complicated by the interference fringes. We therefore sample the cavity output directly in the time domain. For this experiment, port 1 is connected to an RF source generating a fixed frequency f_d gated with a function $G_{\text{in}}(t)$ and port 3 is connected without gating to an oscilloscope that digitizes V_{out} [Fig. 4 (a-b)]. Typical traces averaged over ~ 3500 repetitions are shown in Fig. 4 (c-d) insets. Because the electrical ringdown is close in frequency to the mechanical one, it is not straightforward to separate them in the time domain. Instead, we take a segment of duration t_Δ from each averaged trace and transform it to give a frequency power spectral density (PSD), in which the mechanical signal appears as a separate peak. For

acceptable signal-to-noise, we further average PSD over 1250 traces [Figs. 4 (c-d)].

Figure 4 (e-f) shows two-dimensional maps of PSD plotted as a function of frequency and gate voltage in two gate voltage ranges; one ‘open’ [part of the range in Fig. 2(b-c)] and one ‘closed’ [part of the range in Fig. 3]. After subtracting a background due to purely electrical resonances, the mechanical signal is evident as a gate-dependent peak or dip in PSD.

We calculate Q_M from the linewidth in this PSD. Figure 4(c-d) shows spectral densities at fixed gate voltage settings in open and closed configurations. The mechanical signal is evident as a weak but sharp peak superimposed on a broad background arising from several electrical resonances of the cryostat. The choice of t_Δ is set by a tradeoff; larger t_Δ increases the frequency resolution in the PSD and suppresses the background contribution due to the cavity, but also weakens the mechanical peak by incorporating more of the decay. This tradeoff is illustrated by traces for two choices of t_Δ [Fig. 4 (c-d)]. For an open gate configuration [Fig. 4(c)] the mechanical peak is resolved to a width of $\Delta f_M \approx 0.3$ MHz for $t_\Delta = 3.32$ μ s, allowing the estimate $Q_M = f_M/\Delta f_M \approx 1000$. For the closed gate configuration [Fig. 4(d)] the peak’s width is not resolved and only a lower bound $Q_M \gtrsim 900$ is extracted. In this device there is therefore no evidence that Q_M is limited by tunnel resistance, despite the modest value compared with other clean nanotube devices [13, 17, 29]. Since the sensitivity does not yet allow single-shot readout, this is a lower bound, incorporating dephasing as well as decoherence [15]. Interestingly, Q_M is slightly higher than measured previously for a stamped nanotube [16].

To set this work in context with other implementations [1], we calculate several measures of the optomechanical interaction, using the geometrically estimated coupling capacitance [6]. The vacuum optomechanical coupling $g_0 = 2\pi f_E \frac{\partial f_E}{\partial u} u_{zp}$, which is the cavity shift due to zero-point displacement $u_{zp} = \sqrt{\hbar/4\pi m f_M} \approx 2$ pm, is $g_0 \approx 2\pi \times 0.4$ mHz, where m is the nanotube mass [6, 31]. For typical cavity drive of -38 dBm, we estimate the photon occupation as $n_c \approx 8 \times 10^9$, so that the detuned optomechanical strength is $g_D = \sqrt{n_c} g_0 \approx 2\pi \times 35$ Hz. However, the cavity-nanotube interaction near $f_M = f_E$ is parameterized by a resonant coupling $g_R = \frac{V_G}{V_{ZP}} g_0$, where $V_{ZP} \sim 240$ nV is the zero-point voltage on the cavity electrode. Our parameters imply $g_R \approx 2\pi \times 12$ kHz, so that this coupling dominates [6].

This resonant enhancement might allow quantum-limited measurements in the ground state. In a continuous displacement measurement, the uncertainty principle [32–34] limits the position resolution to $\Delta u_{QL} = \sqrt{2/\ln 3} u_{ZP}$. In a detuned configuration, where measurement is via phase shift to a cavity probe tone, the attainable imprecision at low temperature is typically

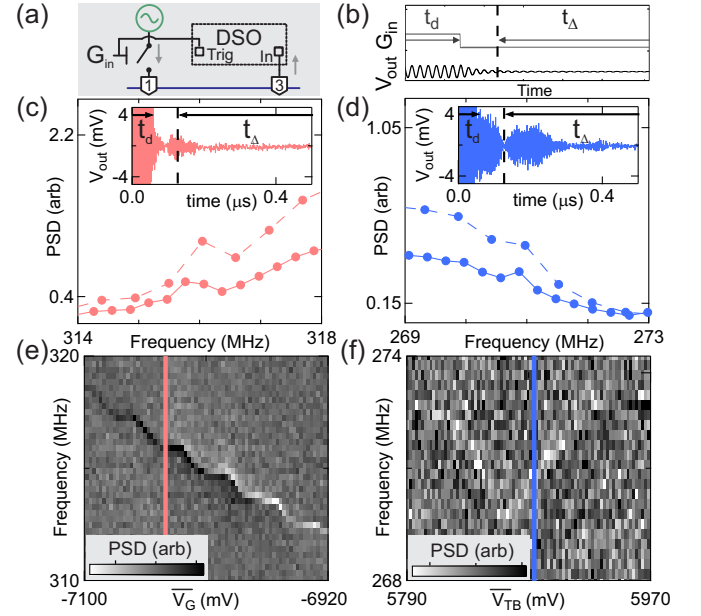


FIG. 4. (a) Gating scheme using a RF switch to gate the drive and a digital sampling oscilloscope (DSO), triggered by the gating signal G_{in} , to capture V_{out} . (b) Schematic of G_{in} and V_{out} . Durations of drive (t_d) and acquisition (t_A) are indicated. (c), (d) Averaged PSD for two fixed gate voltages marked in (e), (f), respectively. Solid (dashed) curves correspond to $t_\Delta = 3.32$ μ s ($t_\Delta = 1.82$ μ s). Measurement parameters were $V_{sd} = 10$ mV, $P = -38$ dBm, $t_d = 330$ ns and time between drive pulses was 3660 ns. For (c), $f_d = 315$ MHz and $V_S = 9$ V, while for (d), $f_d = 273$ MHz and $V_S = 0.2$ V. Insets show averaged V_{out} traces. The drive burst ends ~ 50 ns after the beginning of these traces and acquisition begins ~ 80 ns later (dashed lines). (e), (f) Measured PSD as a function of frequency and gate voltage for the two different device configurations studied, averaged over 65500 repetitions at each gate voltage. A background due to purely electrical resonances was subtracted. The signal-to-noise ratio is better in (e) than in (f), presumably reflecting larger electrical coupling when the nanotube is in a more conducting state.

limited by cavity nonlinearity at high drive power [3]. In our setup, the analog of the probe tone is \bar{V}_G , which does not directly excite the cavity. Given an amplifier voltage sensitivity S_V , Eq. (1) predicts a vibrational amplitude sensitivity $S_u = S_V / (2\pi f_M Z_{trans} \bar{V}_G \frac{\partial C_{CNT}}{\partial u})$, which for our unoptimized parameters is $S_u \approx 6$ pm/ $\sqrt{\text{Hz}}$ [6]. The corresponding imprecision is $\Delta u = S_u \sqrt{\Delta f_M} \approx 1700 \times \Delta u_{QL}$, limited by amplifier noise. To resolve Δu_{QL} would require a near-quantum-limited external amplifier such as a SQUID [35, 36] as well as an increase in Z_{trans} , Q_M , or the coupling strength. With other parameters unchanged, increasing gate length to 550 nm and \bar{V}_G to 65 V would give a quantum backaction imprecision of order Δu_{QL} [6]. This would allow quantum effects to be studied in a resonator near the phonon ground state [6, 37, 38].

We acknowledge discussions with E.M. Gauger and support from EPSRC (EP/J015067/1), DSTL, Marie

Curie CIG and IEF fellowships, the Royal Academy of Engineering, and Templeton World Charity Foundation. The opinions expressed in this publication are those of the authors and do not necessarily reflect the views of Templeton World Charity Foundation. NA performed the experiment. TP developed the fabrication process and contributed to equipment setup. AM fabricated and characterised the device and built the tank circuit. JHW set up the CVD furnace. EAL and NA conceived the experiment and analyzed the data. All authors discussed results and commented on the paper.

-
- [1] M. Aspelmeyer, T. J. Kippenberg, and F. Marquardt, *Rev. Mod. Phys.* **86**, 1391 (2014).
 - [2] S. Gröblacher, K. Hammerer, M. R. Vanner, and M. Aspelmeyer, *Nature* **460**, 724 (2009).
 - [3] C. A. Regal, J. D. Teufel, and K. W. Lehnert, *Nat. Phys.* **4**, 555 (2008).
 - [4] P. A. Truitt, J. B. Hertzberg, C. C. Huang, K. L. Ekinci, and K. C. Schwab, *Nano Lett.* **7**, 120 (2007).
 - [5] T. Bağcı, A. Simonsen, S. Schmid, L. G. Villanueva, E. Zeuthen, J. Appel, J. M. Taylor, A. Sørensen, K. Usami, A. Schliesser, and E. S. Polzik, *Nature* **507**, 81 (2014).
 - [6] See Supplemental Material for details of the simulation, estimate of the single-photon coupling and a discussion of quantum-limited displacement measurements.
 - [7] M. A. Sillanpää, J. Sarkar, J. Sulkko, J. Muhonen, and P. J. Hakonen, *Appl. Phys. Lett.* **95**, 011909 (2009).
 - [8] X. Song, M. Oksanen, M. A. Sillanpää, H. G. Craighead, J. M. Parpia, and P. J. Hakonen, *Nano Lett.* **12**, 198 (2012).
 - [9] V. Sazonova, Y. Yaish, H. Üstünel, D. Roundy, T. A. Arias, and P. L. McEuen, *Nature* **431**, 284 (2004).
 - [10] H. B. Peng, C. W. Chang, S. Aloni, T. D. Yuzvinsky, and A. Zettl, *Phys. Rev. Lett.* **97**, 087203 (2006).
 - [11] B. Witkamp, M. Poot, and H. S. J. van der Zant, *Nano Lett.* **6**, 2904 (2006).
 - [12] B. Lassagne, D. Garcia-Sanchez, A. Aguasca, and A. Bachtold, *Nano Lett.* **8**, 3735 (2008).
 - [13] A. K. Hüttel, G. A. Steele, B. Witkamp, M. Poot, L. P. Kouwenhoven, and H. S. J. van der Zant, *Nano Lett.* **9**, 2547 (2009).
 - [14] E. A. Laird, F. Pei, W. Tang, G. A. Steele, and L. P. Kouwenhoven, *Nano Lett.* **12**, 193 (2012).
 - [15] B. H. Schneider, V. Singh, W. J. Venstra, H. B. Meerwaldt, and G. A. Steele, *Nat. Commun.* **5**, 5819 (2014).
 - [16] A. Benyamini, A. Hamo, S. V. Kusminskiy, F. von Oppen, and S. Ilani, *Nat. Phys.* **10**, 151 (2014).
 - [17] J. Moser, A. Eichler, J. Güttinger, M. I. Dykman, and A. Bachtold, *Nat. Nanotechnol.* **9**, 1007 (2014).
 - [18] K. Jensen, K. Kim, and A. Zettl, *Nat. Nanotechnol.* **3**, 533 (2008).
 - [19] H.-Y. Chiu, P. Hung, H. W. C. Postma, and M. Bockrath, *Nano Lett.* **8**, 4342 (2008).
 - [20] J. Moser, J. Güttinger, A. Eichler, M. J. Esplandiu, D. E. Liu, M. I. Dykman, and A. Bachtold, *Nat. Nanotechnol.* **8**, 493 (2013).
 - [21] C. Ohm, C. Stampfer, J. Splettstoesser, and M. Wegewijs, *Appl. Phys. Lett.* **100**, 143103 (2012).
 - [22] A. Pályi, P. R. Struck, M. S. Rudner, K. Flensberg, and G. Burkard, *Phys. Rev. Lett.* **108**, 206811 (2012).
 - [23] S. Rips, M. Kiffner, I. Wilson-Rae, and M. J. Hartmann, *New J. Phys.* **14**, 023042 (2012), 1104.5665.
 - [24] S. Rips and M. J. Hartmann, *Phys. Rev. Lett.* **110**, 120503 (2013).
 - [25] S. Stapfner, L. Ost, D. Hunger, J. Reichel, I. Favero, and E. M. Weig, *Appl. Phys. Lett.* **102**, 151910 (2013).
 - [26] A. Mavalankar, T. Pei, E. M. Gauger, J. H. Warner, G. A. D. Briggs, and E. A. Laird, arXiv 1603.06278 (2016).
 - [27] N. Ares, F. J. Schupp, A. Mavalankar, G. Rogers, J. Griffiths, G. A. C. Jones, I. Farrer, D. A. Ritchie, C. G. Smith, A. Cottet, G. A. D. Briggs, and E. A. Laird, *Phys. Rev. Applied* **5**, 034011 (2016).
 - [28] S. Sapmaz, Y. M. Blanter, L. Gurevich, and H. S. J. van der Zant, *Phys. Rev. B* **67**, 235414 (2003).
 - [29] G. A. Steele, A. K. Hüttel, B. Witkamp, M. Poot, H. B. Meerwaldt, L. P. Kouwenhoven, and H. S. J. van der Zant, *Science* **325**, 1103 (2009).
 - [30] B. Lassagne, Y. Tarakanov, J. Kinaret, D. Garcia-Sanchez, and A. Bachtold, *Science* **325**, 1107 (2009).
 - [31] M. Poot and H. S. J. van der Zant, *Phys. Rep.* **511**, 273 (2012).
 - [32] C. M. Caves, *Phys. Rev. D* **26**, 1817 (1982).
 - [33] V. B. Braginsky and F. Y. Khalili, *Quantum Measurement* (Cambridge University Press, 1995).
 - [34] M. D. LaHaye, O. Buu, B. Camarota, and K. C. Schwab, *Science* **304**, 74 (2004).
 - [35] J. Clarke and A. I. Braginski, eds., *The SQUID Handbook: Applications of SQUIDs and SQUID Systems* (John Wiley & Sons, 2006).
 - [36] A. A. Clerk, M. H. Devoret, S. M. Girvin, F. Marquardt, and R. J. Schoelkopf, *Rev. Mod. Phys.* **82**, 1155 (2010).
 - [37] J. D. Teufel, T. Donner, M. Castellanos-Beltran, J. Harlow, and K. W. Lehnert, *Nat. Nanotechnol.* **4**, 820 (2009).
 - [38] G. Anetsberger, P. Verlot, E. Gavartin, O. Arcizet, Q. P. Unterreithmeier, E. M. Weig, M. L. Gorodetsky, J. P. Kotthaus, and T. J. Kippenberg, *Phys. Rev. A* **82**, 061804 (2010).